GMR
The Original

TRANSCRIPTOMIC AND FUNCTIONAL PATHWAY ANALYSIS OF ZIKA VIRUS-INDUCED PARALYSIS AND RECOVERY IN A MOUSE MODEL OF GUILLAIN-BARRÉ SYNDROME

Abdallah Rafi[1*], Selma Yilmaz[1]

[1]Department of Medical Biology, Molecular Medicine Program, Near East University, Faculty of Medicine, Nicosia, North Cyprus

ABSTRACT

We analyze how transcriptional programs shift from paralysis to recovery in a ZIKV-linked GBS mouse model using spinal-cord RNA-seq from sham, paralyzed, and recovering groups. Public reads (PRJNA1144966/SRP524499) were QC'd (FastQC/MultiQC), trimmed (Trim Galore; Phred ≥30; length ≥70 bp), then aligned to mouse GRCm39 with STAR; counts by featureCounts; Ensembl release 109; CPM normalization. edgeR quasi-likelihood contrasts (Paralyzed vs Sham; Recovering vs Paralyzed; Recovering vs Sham), thresholds FDR ≤0.05 and $|\log_2 FC| \geq 1$; PCA showed clear stage separation (one sham outlier on PC2 retained). In paralysis, interferon/NF-κB immune mediators (e.g., TNF, IFIT1, ISG15, OASL2, STAT1, CXCL10) are up, while ribosomal/splicing genes are down; recovery attenuates inflammatory signatures and re-expresses neuronal programs. Paralysis enriches immune/viral response; recovering vs paralyzed enriches axonogenesis/synaptic organization; recovering vs sham retains antigen-receptor/immune-synapse signals. GSEA: strong positive enrichment for interferon/NF-κB in paralysis; neurotrophin/cell-adhesion modules in recovery. Paralysis: KEGG/Reactome cytokines, chemokines, complement, FcR→NF-κB/MAPK; Recovery: shift toward GPCR-linked and synaptic signaling, indicating an immune-to-neural transition. A two-phase trajectory emerges: immune injury → resolution/remodeling. Candidate markers: acute (IFIT1, ISG15, CXCL10, STAT1, TNF), resolution (ARG1, MSR1, CLEC4N, IFI30, TGM2), adaptive recovery (PDCD1, CTLA4, CXCR3, CCL5, IL12B, ITGAE). The study outlines a coherent neuroimmune progression from antiviral/inflammatory activation to reparative neuronal remodeling, proposing phase-specific transcriptional signatures for monitoring and potential therapeutic timing.

KEYWORDS: Zika virus; Guillain-Barré syndrome; RNA-seq; Neuroinflammation; Bioinformatics

1.INTRODUCTION

1.1 Zika Virus Infection and Neurological Complications

Zika virus infection is associated with a wide spectrum of complex neurological complications across age groups. There is significant concern about Congenital Zika Syndrome because it causes neurological problems transmitted from the mother to the fetus during pregnancy (Carod-Artal, 2018, Reid et al., 2018). Among the most prominent neurological abnormalities in this syndrome are microcephaly in the newborn and neuronal migration abnormalities, in addition to ocular abnormalities (Carod-Artal, 2018, Reid et al., 2018). The neuropathogenesis of CZS involves ZIKV's preferential infection and induction of apoptosis in human neural progenitor cells, leading to disrupted synaptogenesis and central nervous system development (Carod-Artal, 2018). In adolescents and adults, Guillain–Barré syndrome, an immune-mediated, multifocal neuropathy, is among the most common disorders, with strong epidemiological evidence indicating links between its increased incidence and the presence of congenital Zika virus syndrome (Carod-Artal, 2018, Reid et al., 2018). The effects of Zika virus infection are not limited to Guillain–Barré syndrome and Congenital Zika Syndrome; they may sometimes extend to other neurological manifestations and clinically significant disorders, for example (without limitation) meningitis, encephalitis and myelitis, encephalopathy, and ischemic infarction (Carod-Artal, 2018, Reid et al., 2018). Autonomic dysfunction has also been identified as a potential neurological sequela of ZIKV infection (Carod-Artal, 2018)

1.2 Guillain–Barré Syndrome and Its Association with ZIKV

Guillain–Barré syndrome, comprising a variety of prominent neurological disorders, is strongly and directly associated with Zika virus infection; therefore, it became a major concern for the World Health Organization during widespread outbreaks (Mier-y-Teran-Romero et al., 2018). Between 2013 and 2014, the epidemiological link was first observed during the outbreak in French Polynesia after a substantial rise in incidence (Cao-Lormeau et al., 2016).

In addition, epidemiological data from Latin American and Caribbean countries recorded increasing numbers of Guillain–Barré syndrome cases following Zika virus infection. Recent studies have indicated an increased incidence of Guillain–Barré syndrome after Zika virus infection, with data pointing to approximately 1 to 8 cases per 10,000 recorded infections (Davies et al., 2023).

With respect to the onset time of Guillain–Barré syndrome (GBS) symptoms, the clinical presentation typically occurs within a period ranging from a few days to several weeks after Zika virus infection (Cao-Lormeau et al., 2016, Schafflick et al., 2017, Davies et al., 2023). Current studies and hypotheses on the link between Zika virus and GBS indicate that the underlying mechanism is an immune-mediated response and a direct relationship involving molecular mimicry between Zika virus–related proteins and neural components that play a key role in the disease process (Anaya et al., 2016, Wang et al., 2022). Nevertheless, some reports have detected anti-ganglioside antibodies in patients with Zika-associated GBS; however, the precise antibody signature and the full pathogenic mechanisms of this condition remain incompletely defined and are still under investigation (Davies et al., 2021, Koike et al., 2021).

Postmortem examinations clearly demonstrated marked demyelination in the peripheral nerves, which strongly supports the presence of Guillain–Barré syndrome and its direct association with Zika virus infection, and suggests that the condition is most likely an acute demyelinating neuropathy. Preparedness by countries with a high risk of Zika virus spread is therefore essential and urgent, particularly through increasing intensive care capacity to promptly control and manage the symptoms of Guillain–Barré syndrome that accompany viral outbreaks (Cao-Lormeau et al., 2016).

1.3 Molecular and Transcriptomic Insights into ZIKV Pathogenesis

The complex molecular mechanisms and transcriptomic signatures are part of the pathogenesis of the Zika virus, which has a distinctive ability to evade and mislead the host's immune responses, resulting in cellular damage, particularly to the nervous system. Regarding the sites of Zika virus infection, it occurs in human dermal fibroblasts and epidermal keratinocytes, which in turn trigger profound changes in RIG-I-like receptors. Notably, the virus expresses a specific protein, NS1, which stands against and counteracts these antivirals signaling pathways through a precise mechanism whereby it directly binds to RIG-I and MDA5 to suppress the induction of IFN and IFN-stimulated genes (ISGs) (Kim et al., 2019). To establish and stabilize this infection in the host, the virus employs a biologically refined evasion of innate immunity, which represents the cornerstone for consolidating its presence in the host. The effects of this virus continue to evolve progressively, with well-documented neurotropism and immune dysregulation that can culminate, particularly in specific contexts, in severe neurological sequelae (Berglund et al., 2024). A set of analyses conducted on patients and on certain cell-culture models, such as A549 human lung carcinoma cells, indicated shared patterns of gene expression and alternative splicing; thus, in vitro models can effectively explain the molecular changes observed in patients. These studies present time-resolved patterns of gene expression, cellular profiles, and inflammatory signatures across the stages of infection (Berglund et al., 2024).

In adults, most ZIKV infections are asymptomatic or mild. Severe neurological complications such as Guillain–Barré syndrome and, less commonly, encephalitis occur in a minority of cases but are clinically significant due to potential severity. (By contrast, congenital infection can cause profound brain injury.) The infection targets neural precursor cells, which leads to marked motor and cognitive deficits in affected patients due to its pronounced neurotropism. The virus disrupts the microRNA circuitry by suppressing and downregulating toll-like receptor-3 (TLR3) signaling, and as a result, chronic inflammation develops through the alteration of the host cellular machinery required for viral replication (Bhagat et al., 2021).

In the brain, this pathological state arises because the Zika virus interrupts normal neural development by inducing apoptosis, activating proliferation in progenitor cells, and inhibiting neurogenesis and astrogliogenesis. This is not limited to those mechanisms; the virus also triggers and activates immune cells, most notably microglia and astrocytes, which then secrete proinflammatory cytokines. As with most flaviviruses, entry of the Zika virus into the human host occurs via clathrin-dependent endocytosis with the assistance of the E protein. The severity of ZIKV-associated neuropathology depends on several biological factors, including infection of regenerating brain cell types and of cortical neural progenitors, radial glial cells, and microglial cells (Bhagat et al., 2021). The link between Zika virus infection and Guillain–Barré syndrome is not in doubt; however, the cellular and biological changes that control the transition between the disease states from the paralysis state to the recovery state are still unclear and not sufficiently described to answer the important questions in this condition. Therefore, this study focuses on finding answers about these transitions by using transcriptome and pathway analysis in a mouse model that includes different disease states. This study applies differential gene expression to the three mouse groups in the disease spectrum (sham, paralyzed, and recovering) and then applies tools such as GSEA, GO, and KEGG to determine the functional categories between each group. For the biomarkers and therapeutic targets, we will follow the high-importance genes that show strong links between the paralysis state and the recovery state. In the last part, to determine the biphasic trajectory for full recovery and tissue modelling, we will use a multi-contrast framework (sham vs recovering vs paralyzed).

2.MATERIALS AND METHODS

2.1 Data source and acquisition

Publicly available RNA-seq data from Zika-virus-infected mice were acquired from the NCBI Sequence Read Archive (BioProject PRJNA1144966; SRP524499). This dataset includes spinal-cord tissues from adult Mus Musculus, categorized into three experimental groups: paralyzed, recovering (post-paralytic), and sham (mock-infected controls). Each group consisted of at least three biological replicates (Figure 1). This murine model effectively recapitulates the neuroinflammatory and paralytic phenotypes observed in human ZIKV-associated Guillain–Barré syndrome, thereby enabling a temporal analysis of the transcriptional cascade from viral neuroinvasion to recovery. No new wet-lab experiments were performed in this study; all analyses represent in-silico secondary re-analysis of these open datasets.

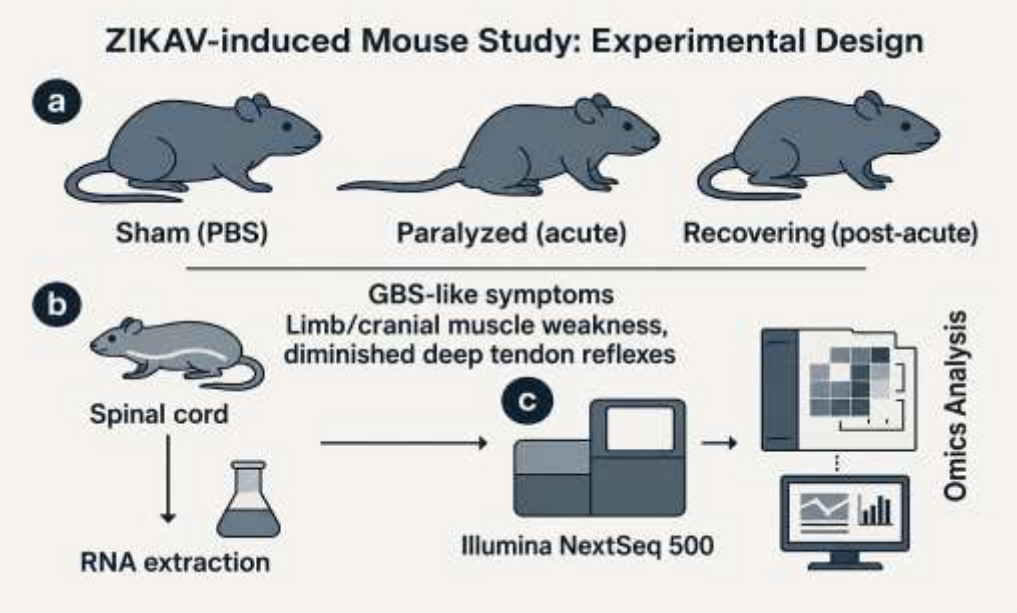

Figure 1 – Zika virus–induced mouse model and spinal cord RNA-seq experimental design

The metadata associated with PRJNA1144966/SRP524499 was reviewed before analysis to confirm sample grouping and evaluate potential confounding variables. The analyzed RNA-seq dataset included 13 spinal-cord samples: six sham-infected, four paralyzed, and three recovering/post-paralytic samples. Available metadata confirmed the use of IFNAR−/− *Mus musculus* on a C57BL/6 background, spinal-cord tissue, single-end Illumina NextSeq 500 RNA-seq, and ZIKV PRVABC59 or sham-infection experimental conditions. The sham group included five male and one female mouse, the paralyzed group included three male and one female mouse, and the recovering group included one male and two female mice. Reported ages ranged from approximately 4.9 to 5.5 months. Disease-stage assignment was based on the original sample annotation as sham-infected, paralyzed, or recovering. Because this was a secondary re-analysis of a modest public RNA-seq dataset, sex, age, and collection timing were reviewed as potential confounders but were not included as covariates in the differential-expression model to avoid overfitting. Therefore, the results should be interpreted as disease-stage-associated transcriptional signatures rather than fully covariate-adjusted causal effects.

2.2 Transcriptomic Data Processing and Quality Control

Raw FASTQ files were downloaded via SRA Toolkit 3.1.1 to local storage and inspected for quality using FastQC v0.11. and MultiQC v1 (SRA Toolkit Archives, 2021, Babraham Bioinformatics, n.d., Seqera, n.d.). Low-quality bases and adapter sequences were trimmed with Trim Galore! v0.6.7, retaining reads with Phred ≥ 30 and length ≥ 70 bp. Per-sample statistics, including read counts, GC content, and duplication rates, were summarized to ensure uniform sequencing depth across all samples (Krueger et al., 2023). Raw gene-level counts were filtered to remove low-abundance genes by retaining genes with counts per million (CPM) >1 in at least two libraries. For differential-expression analysis, raw count data were analyzed in edgeR using trimmed mean of M-values (TMM) normalization to account for library-size and composition differences. CPM/$\log_2$CPM values were used only for filtering, exploratory principal component analysis, heatmaps, and visualization, not as the input scale for the statistical differential-expression model. QC included principal component analysis (PCA) on stabilized counts and inspection of library-size distributions. One sham replicate exhibited modest deviation on PC2 but remained within group variance; all samples were retained. Multiple testing was controlled with Benjamini–Hochberg FDR (Benjamini and Hochberg, 1995, Robinson et al., 2010, Dobin et al., 2013, Liao et al., 2014).

2.3 Read Alignment and Quantification

Clean reads were aligned to the mouse reference genome GRCm39 using STAR v2.7.10a with default two-pass mapping and gene-level quantification via featureCounts v2.0.3 (Dobin et al., 2013, Liao et al., 2014). Gene annotations were derived from Ensembl release 109. The resulting raw integer count matrix was consolidated across all samples and retained for downstream differential-expression analysis. TMM normalization factors were estimated within edgeR for statistical modeling, whereas CPM/$\log_2$CPM values were generated for filtering, quality-control assessment, and visualization.

2.4 Differential Gene Expression Analysis

Group-wise contrasts, Paralyzed vs Sham, Recovering vs Paralyzed, and Recovering vs Sham, were evaluated using edgeR v3.42.4 (Robinson et al., 2010). Genes with CPM >1 in at least two libraries were retained. TMM normalization was applied in edgeR before dispersion estimation and quasi-likelihood model fitting. Differential expression was assessed using empirical Bayes moderated quasi-likelihood F-tests. Significance thresholds were set at FDR ≤0.05 and $|\log_2 FC| \geq 1$. Volcano plots and heatmaps were generated from normalized $\log_2$CPM values using ggplot2 v3.4.4 and pheatmap v1.0.12 in R 4.3 (Wickham, 2009, Kolde, 2010).

2.5 Functional Annotation and Gene Ontology Mapping

First, the significant DEGs were annotated by integrative matching of Ensembl gene IDs with official gene symbols, in addition to all functional descriptions in Ensembl BioMart, using Mus musculus GRCm39. All available GO categories were used, namely Biological Process (BP), Molecular Function (MF), and Cellular Component (CC), along with Fisher's exact test and an FDR ≤ 0.05 (Thomas et al., 2022).

2.6 Pathway Enrichment and Gene Set Enrichment Analysis

To identify the pathways that were overrepresented in the significant DEGs, ORA was applied first. After that, to provide a complementary description, GSEA was performed to characterize pathway-level changes across the full gene-ranking spectrum. The combined use of both approaches increases confidence in the cellular pathways, particularly immune and metabolic pathways, that appear repeatedly in the results of both methods (Subramanian et al., 2005). The pathway enrichment workflow presented in Table 1.

Table 1. Pathway enrichment workflow

Step / Stage	Method / Tool	Parameters / Criteria	Output
Stage 1: Pathway over-representation	ORA with KEGG and Reactome	Fisher's exact test, FDR ≤ 0.05	Statistically enriched pathways among significant DEGs
Stage 2: Gene set–level enrichment	GSEA on full ranked list (by $\log_2$FC)	1,000 permutations; significance: NES, FDR q ≤ 0.25	Positively/negatively enriched gene sets
Visualization	bubble plots, enrichment maps via GSEA + ggplot2	—	Graphical representation of enriched pathways

ORA: Over-representation analysis, KEGG: Kyoto Encyclopedia of Genes and Genomes, GSEA: Gene Set Enrichment Analysis, $\log_2$FC: Log2 fold change, FDR: False discovery rate, NES: Normalized enrichment score, DEGs: Differentially expressed genes.

2.7 Statistical Analysis

All statistical analyses were performed in R v4.3. Differential gene expression across the three contrasts was evaluated using edgeR v3.42.4 with a quasi-likelihood framework and empirical Bayes moderation. The edgeR statistical model was fitted to raw gene-level counts with TMM normalization factors; CPM/$\log_2$CPM values were used only for filtering, exploratory analysis, and visualization, and multiple testing was controlled using the Benjamini–Hochberg false discovery rate (FDR). Genes were considered differentially expressed at FDR ≤ 0.05 with $|\log2FC| \geq 1$. For functional interpretation, Gene Ontology and pathway over-representation analyses used Fisher's exact test with FDR ≤ 0.05, and gene set enrichment analysis (GSEA) was performed on the full ranked list (by log2FC) using 1,000 permutations, reporting normalized enrichment scores (NES) and considering FDR q ≤ 0.25 significant.

2.8 Ethical Concerns

This study was conducted using publicly available, de-identified human-related datasets accessed from open research repositories. No new data was collected, and the authors had no direct interaction with human participants or access to identifiable personal information. Therefore, informed consent was not required, and ethical approval from an institutional review board or ethics committee was not necessary for this study.

3.RESULTS

3.1 Quality Control and Sample Clustering

In Figure 2, we can observe distinct clusters for sham, paralyzed, and recovering. PCA of standardized counts showed a clear separation along PC1 (52% of the variance). Recovering samples were positioned intermediate relative to the

paralyzed samples. The plot in Figure 3 shows the library-size distribution between 18–49 million reads per sample used in the experiment, underscoring the importance of library-size normalization. One sham replicate showed partial deviation along PC2; however, it was retained because it did not show evidence of technical failure, had an acceptable library size, and did not drive the major disease-stage separation observed along PC1, which explained 52% of the variance. Because PC1 captured the dominant biological separation among sham, paralyzed, and recovering groups, the PC2 deviation was interpreted as limited within-group variation rather than a sufficient basis for exclusion. Therefore, all biological replicates were retained for the final differential-expression analysis to avoid introducing subjective sample-removal bias.

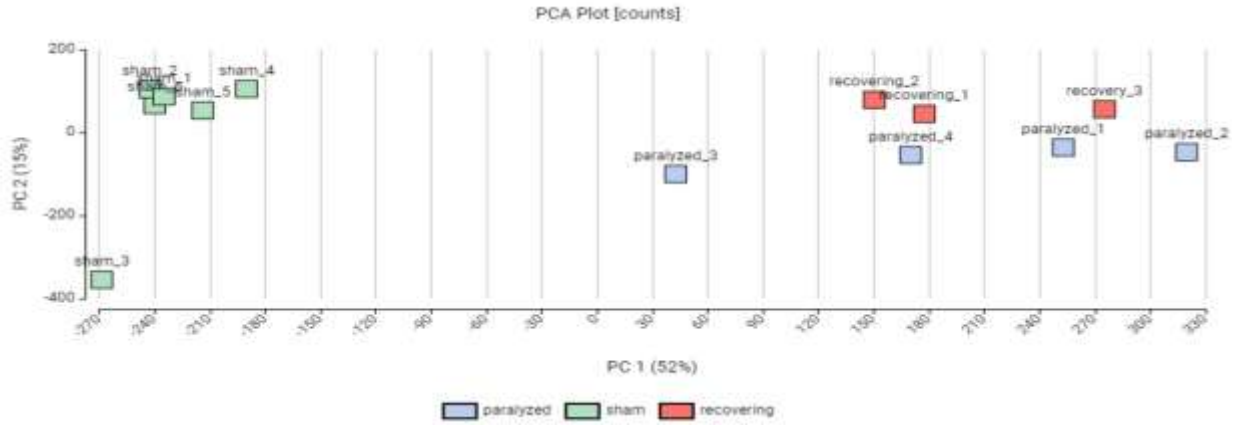

Figure 2 – Principal component analysis of sham, paralyzed, and recovering spinal cord transcriptomes

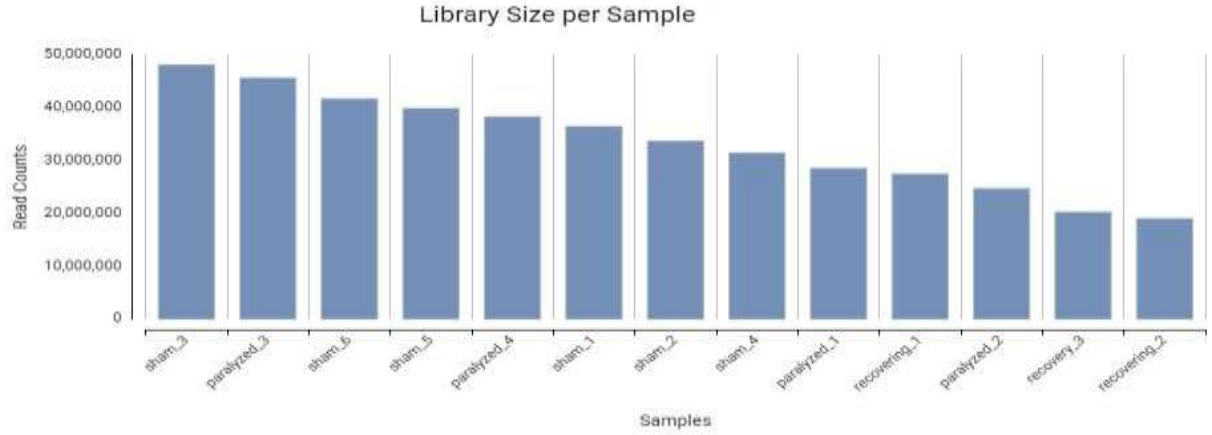

Figure 3 – RNA-seq library size distribution across sham, paralyzed, and recovering samples

3.2 Differentially Expressed Genes Across Contrasts

edgeR analysis identified 2,137 significant DEGs (FDR ≤ 0.05, $|\log_2 FC| \geq 1$) across the three contrasts. Paralyzed vs Sham: 1,142 upregulated and 995 down-regulated genes (Figure 4). Recovering vs Paralyzed: 728 genes with attenuated immune/inflammatory signatures and re-expression of neuronal genes (Figure 5). Recovering vs Sham: 412 differential genes retaining checkpoint and synaptic reorganization signatures (Figure 6). Volcano plots illustrate symmetrical distributions of large-effect DEGs, while the top 50 ranked genes capture the most statistically salient features based on FDR and $|\log_2 FC|$. In the comparison of paralyzed versus sham, notable upregulated immune mediators include Tnf, Ifit1, Oasl2, Stat1, Isg15, and Cxcl10, canonical interferon-stimulated genes (ISGs) implicated in the flaviviral response (Lazear et al., 2016, Ricklin et al., 2016). Down-regulated features included rpl and rps ribosomal families and splicing-associated genes (SF3B1, SRSF3), consistent with transient suppression of translation and RNA metabolism during acute injury (Miner and Diamond, 2017). The recovering contrasts show partial normalization of these patterns, highlighting reversal of inflammatory transcriptional states.

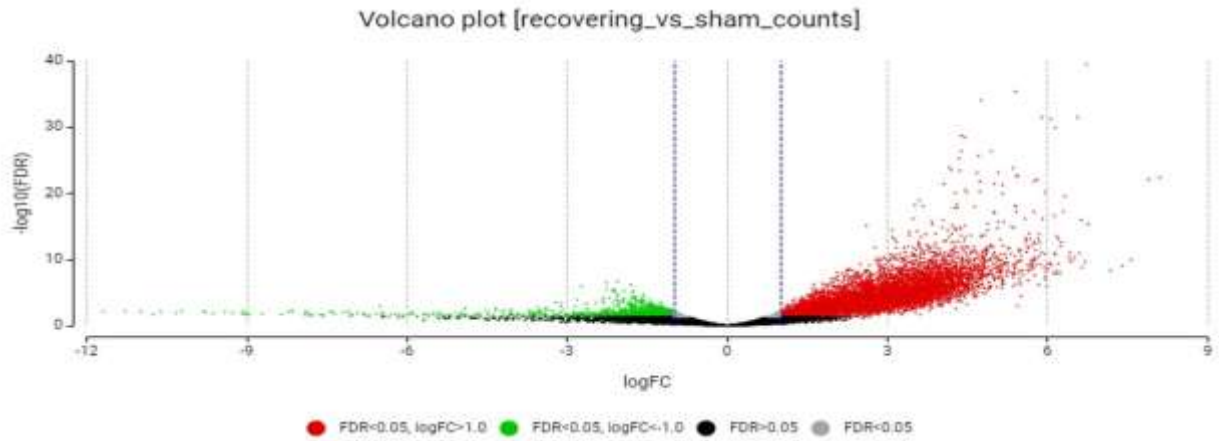

Figure 4 – Volcano plot of differentially expressed genes in recovering versus sham spinal cords

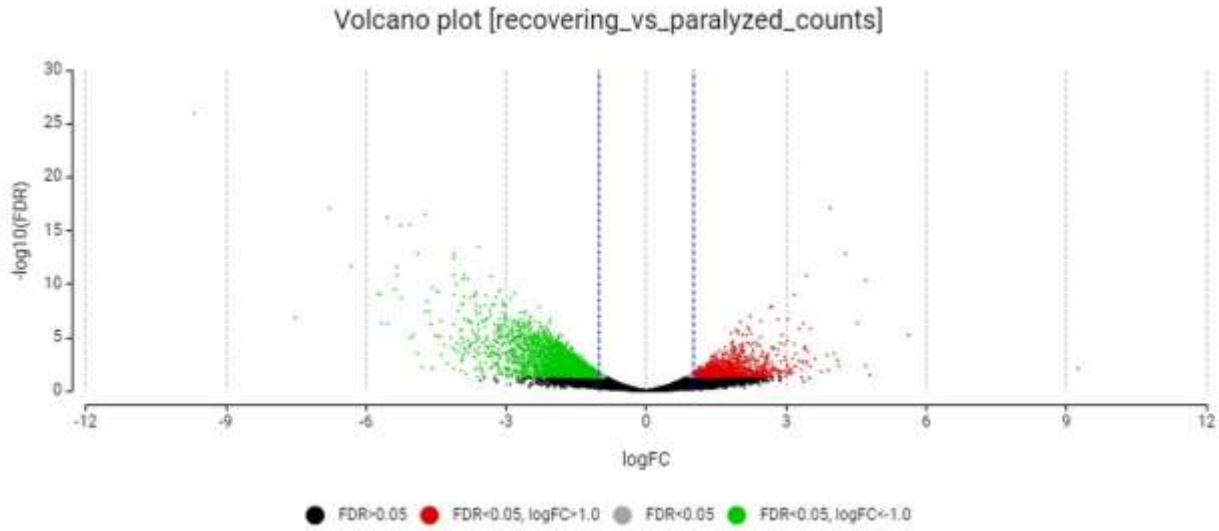

Figure 5 – Volcano plot of differentially expressed genes in paralyzed versus sham spinal cords

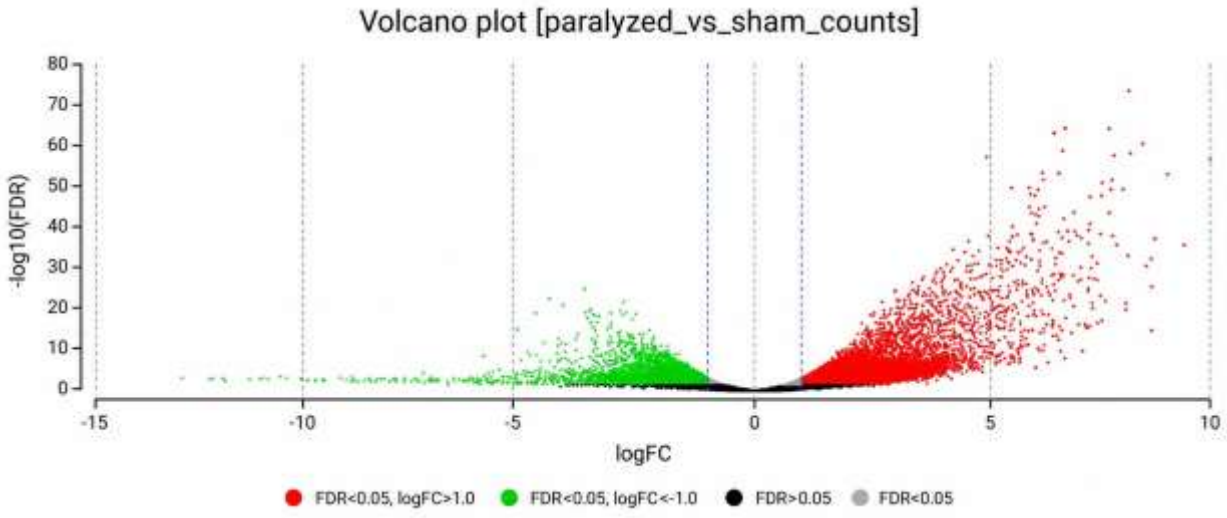

Figure 6 – Volcano plot of differentially expressed genes in recovering versus paralyzed spinal cords

3.3 Heatmap Visualization of Top Differentially Expressed Genes

The clustered heatmaps in each contrast showed clearly distinct expression patterns for each stage for the top DEGs. A clear upregulation of immune-related genes was observed, represented by TNF, IFIT1, ISG15, OAS2, CXC19, and

STAT1 in addition to cytokines in the paralyzed samples. In contrast, in the recovering samples, a restoration of metabolic and structural/cytoskeletal gene expression was observed, represented by GAP43, TUBB, and ACTB. Hierarchical clustering separated the samples according to disease stage, indicating and confirming biological reproducibility. These patterns in the heatmaps and the immune and regenerative signatures are derived from the volcano plots.

3.4 Functional Enrichment by Gene Ontology

Table 2 presents a gradual clarification, starting with the comparison of paralyzed vs sham, which shows acute immune activation. As for the comparison of recovering vs paralyzed samples, it shows Neuronal growth and network organization. Finally, for the comparison of recovery vs sham, the comparison shows persistent immune signaling, which serves as evidence of ongoing immune–neural crosstalk. Overall, these results, as clearly shown in the table, support a biphasic trajectory: early inflammation followed by a repair phase and then structural recovery (Ashburner et al., 2000).

Table 2. GO Enrichment Summary Across Contrasts (FDR ≤ 0.05)

Contrast	Direction/Signal	Enriched GO terms (FDR ≤ 0.05)
Paralyzed vs Sham	Enrichment	"immune system process"; "response to virus"; "cytokine-mediated signaling pathway"
Recovering vs Paralyzed	Up-ranking	"axonogenesis"; "synaptic organization"; "cellular response to growth factor stimulus"
Recovering vs Sham	Persistent signals	"antigen receptor signaling"; "immune synapse assembly"

GO: Gene Ontology, FDR: False discovery rate, FDR: False discovery rate.

3.5 Gene Set Enrichment Analysis (GSEA) of Biological Processes

Ranked-based GSEA revealed pathways with a positive enrichment profile (NES = 3.21, $p < 0.001$), particularly in the interferon alpha/beta response pathway, and pathways related to NF-κB–dependent cytokine pathways (Subramanian et al., 2005). On the other side of the disease phase (paralysis), pathways with a negative profile appeared (NES = −2.74, $q < 0.01$). In the recovery phase, neurotrophin signaling and cell-adhesion pathways clearly emerged as positively enriched modules, which strongly indicates synaptic remodelling and axon extension. These findings are consistent with the heatmaps and volcano results for the two-phase transcriptomic trajectory.

3.6 Pathway Enrichment Analysis (ORA and GSEA)

Phase-dependent remodeling appeared in the signaling associated with the paralyzed stage. As shown in Table 3, a dominant inflammatory–immune program was present, characterized by cytokines, chemokines, and complement, and it activated NF-κB/MAPK through Fc-receptors, which is fully consistent with a strong innate–adaptive crosstalk (Kanehisa, 2000). In the recovery phase, enrichment was clearly shifted toward GPCR-linked and synaptic pathways, which strongly supports the occurrence of a coordinated immune–neural switch, indicating a clear decline in infection level and a transition from the defense phase to repair, and finally to functional restoration (Lazear et al., 2016, Jassal et al., 2019, Leonhard et al., 2019).

Table 3. Immune and neuronal pathways enriched across paralysis and recovery phases

Source / Analysis	Condition (Contrast)	Upregulated / Enriched Pathways	Interpretation
KEGG	Paralyzed vs Sham	Cytokine–cytokine receptor interaction; Chemokine signaling; Complement cascades	Strong innate–adaptive interface activation (inflammatory/antiviral response)
Reactome	Paralyzed vs Sham	FcγR / FcεRI → NF-κB / MAPK; Complement activation; B-cell receptor (BCR) signaling	Fc-receptor–driven immune activation and humoral signaling during paralysis
Reactome	Recovering vs Paralyzed	GPCR-linked pathways; Synaptic/neural signaling pathways	Shift from immune activation to neuronal/synaptic remodeling during recovery

KEGG: Kyoto Encyclopedia of Genes and Genomes, FcγR: Fc gamma receptor, FcεRI: High-affinity IgE Fc receptor I, NF-κB: Nuclear factor kappa B, MAPK: Mitogen-activated protein kinase, GPCR: G protein–coupled receptor.

3.7 Mechanistic Interpretation: Key Pathways Underlying Paralysis and Recovery

A coherent two-phase trajectory is evident. Looking at the first phase, paralyzed vs sham, in the immune injury stage, there is up-regulation of genes closely linked to interferon-stimulated pathways and NF-κB genes, which fundamentally drive neuroinflammation and neural stress. In the second phase, recovering vs paralyzed (resolution and remodeling phase), the process reflects a repair stage, mainly through attenuation of inflammatory axes together with up-regulation of cytoskeletal and synaptic genes. From a biological perspective, this progression mirrors the

clinical stages of recovery from Guillain–Barré syndrome and opens the way to highlight a set of potential biomarkers: CXCR3, ARG1, NOS2, PDCD1, CTLA4, IL12B (Cao-Lormeau et al., 2016, Leonhard et al., 2019).
Looking at the Figures below, the protein–protein interaction network from the paralyzed vs sham contrast shows a tightly connected interferon–inflammation module that is centrally organized around STAT1, with dense links to CXCL10, IFIT1, ISG15, OASL2, and TNF (Figure 7). The topology indicates coordinated activation of type I/II interferon signaling pathways, antiviral effector programs, and chemokine-driven leukocyte trafficking, in clear agreement with the biological patterns seen in the volcano/heatmap and with the GO: BP enrichment terms "response to virus," "type I interferon signaling," and "cytokine-mediated signaling." The strong connectivity of STAT1 and TNF confirms that these two nodes function as organizational hubs, integrating upstream sensing with downstream transcriptional and inflammatory cascades, which point to and support an acute neuroimmune injury phase.

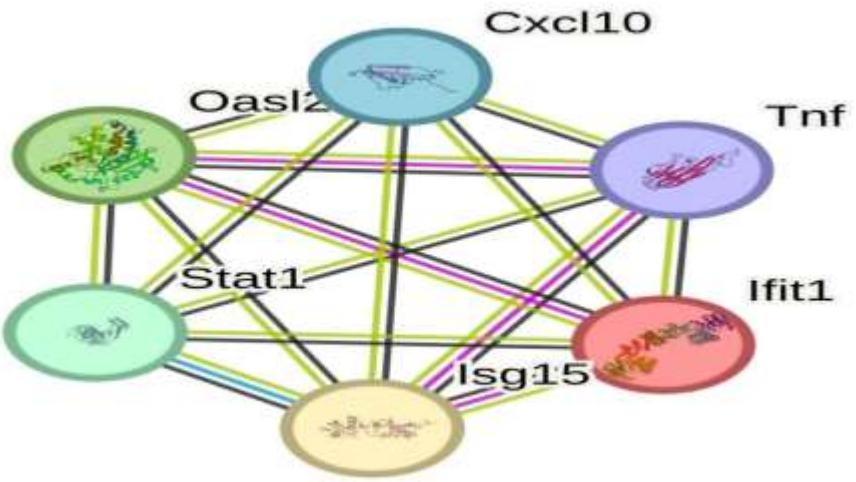

Figure 7 – Protein–protein interaction network of core antiviral and inflammatory hub genes

The observed network architecture shows biological programs related to efferocytic clearance and lipid handling (ARG1 / MSR1 / MRC1), to pattern recognition and antigen processing (CLEC4N / IFI30), and to extracellular matrix cross-linking/remodeling (TGM2), all of which collectively indicate macrophage repolarization toward a reparative phenotype (Figure 8). Accordingly, the network structure supports the transcriptomic transition from inflammatory injury to resolution, in alignment with the enrichment in phagocytosis, endo-lysosomal processing, and extracellular matrix organization.

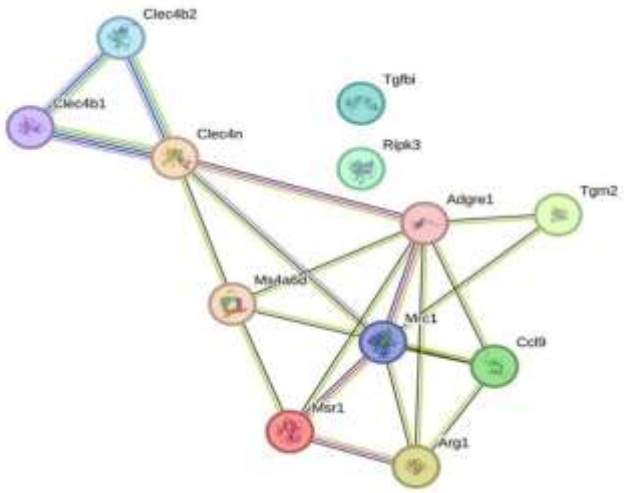

Figure 8 – Protein–protein interaction network of monocyte/macrophage and microglial remodeling genes

In the recovery phase, the biomarker network shows an adaptive/checkpoint signature composed of the proteins PDCD1, CTLA4, CXCR3, CCL5, IL12B, and ITGAE (Figure 9). These interactions among the nodes confirm the

persistence of T-cell regulation and trafficking: IL12B supports Th1/cytotoxic polarization, the CXCR3–CCL5 axis indicates recruitment/retention of effector cells, while ITGAE points to the presence of tissue-resident memory T-cell niches. PDCD1/CTLA4 represents checkpoint engagement in a manner consistent with a controlled immune tone during recovery. This small, precise, and coherent module supports the interpretation that a modulated adaptive immune program remains active at the same time that neural tissues are undergoing remodelling and function is returning to the pre-disease state.

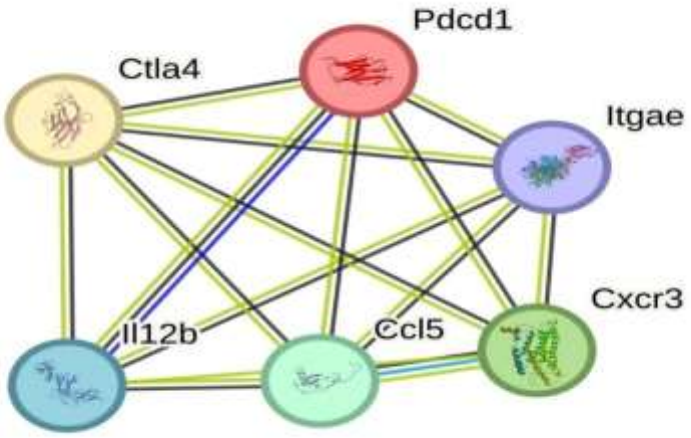

Figure 9 – Protein–protein interaction network of recovery-associated T-cell checkpoint and chemokine genes

4. DISCUSSION

4.1 Paralyzed vs Sham: Neuroimmune Activation and Translational Arrest

The acute phase of the disease is represented by paralyzed vs sham, in which ZIKV infection triggers broad neuroimmune activation. The transcriptomic profile is dominated by upregulation of interferon-stimulated genes (ISGs) ISG15, OASL2, STAT1, CXCL10, TNF, together with NF-κB–dependent cytokines, confirming a strong innate antiviral signaling response. Enrichment analyses in both KEGG and Reactome identified dense and characteristic activation of cytokine–cytokine receptor interaction, chemokine signaling, FcγR/FcεRI → NF-κB/MAPK, and complement activation pathways, the mechanistic features of inflammation and immune-mediated axonal injury (Kanehisa, 2000, Ricklin et al., 2016, Jassal et al., 2019).

Functionally, these modules match a strong innate–adaptive crosstalk: FcR engagement and complement opsonization promote phagocytosis and antigen presentation, while interferon responses reduce viral replication but at the same time increase neurotoxicity (Kanehisa, 2000, Ricklin et al., 2016, Jassal et al., 2019). Likewise, downregulation of ribosomal and spliceosomal genes provides evidence of suppression in translation and general transcription, a pattern frequently observed in virally infected neurons undergoing stress and metabolic reprogramming. GSEA results further confirmed strong positive enrichment for the pathways "response to virus," "immune effector process," and "interferon alpha/beta signaling" (NES > 3.0, FDR < 0.001) alongside negative enrichment for "ribosome biogenesis" and "RNA processing" (NES < −2.0, FDR < 0.01). Taken together, these patterns depict an immune-injury phase in which antiviral defense dominates at the expense of neuronal homeostasis. These transcriptomic signatures point to early events and primary mechanisms in the pathogenesis of Guillain–Barré syndrome (GBS), whereby both molecular mimicry and aberrant immune activation contribute to demyelination and paralysis (Cao-Lormeau et al., 2016, Leonhard et al., 2019). Genes such as STAT1, ISG15, OAS1A, and CXCL10 can therefore serve as biomarkers of acute ZIKV neuroinflammatory burden, since they simultaneously reflect infection-driven immune signaling and collateral neuronal stress.

4.2 Immune and Inflammatory Pathways Driving Neurological Dysfunction

The down-ranking of ribosome/spliceosome pathways, clearly observed both in the negatively valued features from the volcano analysis and in the GSEA sets that were less active, indicates a transcriptional economy under inflammatory pressure, a well-known feature of acutely and severely injured neural tissue (Miner and Diamond, 2017). The pathway panels (KEGG/Reactome) and rank-based GSEA consistently show the pathways cytokine–cytokine receptor interaction, chemokine signaling, FcγR/FcεRI → NF-κB/MAPK, and complement activation during the paralysis phase. These modules collectively constitute myeloid activation, opsonization, and antigen presentation, in line with canonical antiviral defense and neuroinflammation (Kanehisa, 2000, Hayden and Ghosh, 2008 Ricklin et al., 2016, Jassal et al., 2019).

4.3 Paralyzed vs Recovering: Resolution Biology and Myeloid Repolarization

The contrast between paralyzed and recovering captures the transition from inflammatory injury to resolution and tissue repair. Compared with the paralyzed state, recovering samples show downregulation of proinflammatory mediators such as NOS2, IL4RA, and TNF, together with upregulation of genes closely related to phagocytosis, lipid metabolism, extracellular matrix remodeling, and antigen processing, namely: MSR1, CLEC4N, IFI30, ARG1, TGM2, CCL9, RIPK3, and TGFBI. Reactome and KEGG enrichment results provide strong evidence for attenuation of cytokine-driven signaling and for the emergence of GPCR-linked chemosensory modules (repositories similar to olfactory-like receptor repertoires) that frequently co-occur with neuronal remodeling in murine tissues (Kanehisa, 2000). Complement of regulators and Fc receptor–linked components remain expressed at modest/basal levels, indicating the presence of residual immune monitoring without active tissue injury.

From a cellular viewpoint, this shift reflects repolarization of macrophages and microglia from the M1 ($NOS2^+$, inflammatory) phenotype to the M2 ($ARG1^+$, reparative) phenotype, thereby supporting clearance of myelin debris and promoting axonal regrowth (Nimmerjahn and Ravetch, 2008, Ricklin et al., 2016). MSR1 (macrophage scavenger receptor) and CLEC4N (C-type lectin) mediate apoptotic-cell and pathogen debris clearance, whereas IFI30 (gamma-interferon-inducible lysosomal thiol reductase) contributes to antigen processing and redox regulation.

GSEA patterns clearly underscore this resolution phase, with up-enrichment of the pathways “cell adhesion”, “axonogenesis”, and “extracellular structure organization”, and, on the other hand, down-enrichment of “interferon response” and “inflammatory mediator regulation of TRP channels”. These findings define a transcriptomic inflection point representing a cellular transition from immune amplification to repair and neuroprotection (Nimmerjahn and Ravetch, 2008, Ricklin et al., 2016).

From a biological perspective, this stage represents spinal-cord immune rebalancing following gradual viral clearance, and during this phase, there is co-normalization of both neuronal excitability and myeloid activation. This stage leads to narrowing down the selection of the best candidate biomarkers, such as ARG1, MSR1, CLEC4N, and IFI30, which reflect this adaptive resolution, and may substantially aid in defining the therapeutic timing for immunomodulatory interventions.

4.4 Recovering vs Sham: Persistent Adaptive Footprints and Synaptic Remodeling

The pairwise comparison of recovering vs sham shows that, even with the gradual resolution and disappearance of inflammation, a residual adaptive immune signature remains traceable. Among the genes that exhibited marked up-regulation were immune checkpoint genes such as PDCD1 and CTLA4, T-cell receptor (TCR) signaling components such as CD3D, TRBC1, SKAP1, chemokines such as CCL5 and CXCR3, in addition to co-stimulatory ligands such as CD40LG and IL12B. On close examination of the functional enrichment analysis results, we observe sustained activation of the cellular pathways “antigen receptor signaling,” “immune synapse assembly,” and “cell–cell adhesion” within GO: BP, which indicates that memory T cells and tissue-resident lymphocytes remain present within the spinal cord neural tissue even after clinical recovery (Leonhard et al., 2019). The presence of ITGAE (CD103) further supports this conclusion, as it represents a strong biological marker of tissue-resident memory T cells that maintain local immune surveillance (Nimmerjahn and Ravetch, 2008). The adaptive immune footprint coincides with the upregulation of genes related to neuronal repair and synaptic pathways, represented by the gene set GAP43, TUBB3, and SYT1. This sustained immune tone indicates the occurrence of neuroregeneration. On the other hand, the dual presence of both neuronal transcripts and immune transcripts clearly ensures the existence of a balance between several biological factors, particularly immune vigilance after ZIKV neuropathogenesis. It is also notable that, in human GBS, similar residual immune signatures have been detected during clinical remission, which leads to a slowing of transcriptional recovery compared with electrophysiological normalization (Cao-Lormeau et al., 2016, Leonhard et al., 2019). These findings clearly demonstrate the diagnostic potential of PDCD1, CTLA4, and the CXCR3/CCL5 axis as phase-specific immuno-monitoring biomarkers, and they also point to the possibility that modulating checkpoint signaling may influence recovery kinetics.

4.5 Integrative Perspective: A Unified Model of Paralysis and Recovery

The three contrasts together represent a coherent temporal program in which ZIKV-induced neuroinflammation is followed by a recovery phase. This consistent, phased pattern reflects the clinical evolution of GBS, which is characterized first by immune injury, then resolution, and finally functional restitution (Leonhard et al., 2019). This, in turn, supports a coherent neuroimmune plasticity model in which the innate, adaptive, and neuronal programs alternate in dominance and then return to baseline over time.

4.6 Biomarker and Vaccine-Relevant Implications

The molecular transitions in Table 4 reveal biologically anchored candidate biomarkers across the different disease stages: In the acute immune injury phase: IFIT1, ISG15, CXCL10, STAT1, TNF; in the resolution phase: ARG1, MSR1, CLEC4N, IFI30, TGM2; in the adaptive recovery phase: PDCD1, CTLA4, CXCR3, CCL5, IL12B, ITGAE.

From a translational point of view, these markers define measurable transcriptional signatures for monitoring disease trajectory and the recovery phase in post-viral neuropathies. However, while host genes alone are not considered vaccine targets, their network topology provides information on correlates of protection and on optimal adjuvant selection favoring balanced and well-controlled Th1–Th2 responses and regulated checkpoint activity (Kanehisa, 2000, Mier-y-Teran-Romero et al., 2018).

Table 4: Phase-specific candidate biomarkers

Phase	Dominant transcriptomics features	Biological interpretation
Paralyzed vs Sham	Up: ISGs, NF-κB cytokines, Fc/complement. Down: ribosome/spliceosome.	Antiviral and inflammatory injury; transcriptional economy.
Paralyzed vs Recovering	Up: ARG1/NOS2 balance, MSR1, CLEC4N, IFI30.	Myeloid repolarization, debris clearance, and resolution biology.
Recovering vs Sham	Up: PDCD1, CTLA4, CD3D, CXCR3, IL12B, ITGAE.	Residual adaptive footprint, synaptic remodeling, and tissue homeostasis.

ISG: Interferon-stimulated genes, NF-κB: Nuclear factor kappa B.

4.7 Study Limitation: Our study used a single mouse model and viral strain, which may limit generalizability to other systems or human ZIKV-associated GBS. The modest sample size, bulk RNA-seq, and limited time points may have missed subtle or cell-type-specific transcriptional changes. As a primarily observational transcriptomic analysis, we also lack functional and protein-level validation of the candidate genes and pathways. The modest number of biological replicates may limit statistical power for detecting subtle or highly variable gene-expression changes, and the limited sample size prevented formal adjustment for sex, age, or exact collection timing without overfitting.

5.CONCLUSION

By conducting this study on the dynamic transcriptomic landscape of Zika virus–induced paralysis and its recovery, using a laboratory mouse model that mimics the disease state of Guillain–Barré syndrome associated with infection by the coronavirus, the study demonstrated that the paralytic phase was clearly characterized by both antiviral and inflammatory activation, accompanied by suppression of protein synthesis. In contrast, in the resolution phase in the pairwise comparison, paralyzed vs recovering, the study found strong evidence of myeloid repolarization and neuroimmune reprogramming. On the other hand, the convalescent phase resulting from the comparison recovering vs sham retained a moderate adaptive footprint in parallel with synaptic and axonal remodeling. All these results together establish a multi-stage neuroimmune framework that links the pathological stages of ZIKV pathogenesis with the GBS-like recovery phase. The study presented a set of biomarkers suitable for future temporal monitoring, in addition to providing mechanistic anchors that can support immunomodulatory studies and research focusing on producing vaccines in in silico vaccine-design laboratories. To obtain more definitive results, these findings can be validated using single-cell transcriptomics analysis and proteomics to confirm the reliability of these results and make them more suitable for therapeutic targets and immune monitoring strategies.

ACKNOWLEDGEMENTS

The authors thank Benay Buse Çetin for her early presentation, which helped inspire the conceptual development of this study.

REFERENCES

1. Anaya JM, Ramirez-Santana C, Salgado-Castaneda I, Chang C, et al. (2016). Zika virus and neurologic autoimmunity: the putative role of gangliosides. BMC Med. 14: 49.
2. Ashburner M, Ball CA, Blake JA, Botstein D, et al. (2000). Gene Ontology: tool for the unification of biology. Nat. Genet. 25: 25-29.
3. Babraham Bioinformatics (n.d.). FastQC: a quality control tool for high throughput sequence data. Available at [https://www.bioinformatics.babraham.ac.uk/projects/fastqc/].
4. Benjamini Y and Hochberg Y (1995). Controlling the false discovery rate: a practical and powerful approach to multiple testing. J. R. Stat. Soc. Series B Stat. Methodol. 57: 289-300.
5. Berglund G, Lennon CD, Badu P, Berglund JA, et al. (2024). Transcriptomic signatures of Zika virus infection in patients and a cell culture model. Microorganisms. 12: 1499.
6. Bhagat R, Kaur G and Seth P (2021). Molecular mechanisms of zika virus pathogenesis: an update. Indian J. Med. Res. 154: 433-445.
7. Cao-Lormeau VM, Blake A, Mons S, Lastère S, et al. (2016). Guillain-Barré syndrome outbreak associated with Zika virus infection in French Polynesia: a case-control study. Lancet. 387: 1531-1539.
8. Carod-Artal FJ (2018). Neurological complications of Zika virus infection. Expert Rev. Anti-Infect. Ther. 16: 399-410.
9. Davies AJ, Lleixà C, Siles AM, Gourlay D, et al. (2021). Guillain-Barré syndrome following Zika virus infection is associated with a diverse spectrum of peripheral nerve reactive antibodies. medRxiv. Available at [https://doi.org/10.1101/2021.10.28.21265167].

10. Davies AJ, Lleixà C, Siles AM, Gourlay DS, et al. (2023). Guillain-Barré syndrome following Zika virus infection is associated with a diverse spectrum of peripheral nerve reactive antibodies. Neurol. Neuroimmunol. Neuroinflamm. 10: e200047.
11. Dobin A, Davis CA, Schlesinger F, Drenkow J, et al. (2013). STAR: ultrafast universal RNA-seq aligner. Bioinformatics. 29: 15-21.
12. Hayden MS and Ghosh S (2008). Shared principles in NF-κB signaling. Cell. 132: 344-362.
13. Jassal B, Matthews L, Viteri G, Gong C, et al. (2019). The Reactome pathway knowledgebase. Nucleic Acids Res. 2019: gkz1031.
14. Kanehisa M (2000). KEGG: Kyoto encyclopedia of genes and genomes. Nucleic Acids Res. 28: 27-30.
15. Kim JA, Seong RK, Son SW and Shin OS (2019). Insights into ZIKV-mediated innate immune responses in human dermal fibroblasts and epidermal keratinocytes. J. Invest. Dermatol. 139: 391-399.
16. Koike H, Chiba A and Katsuno M (2021). Emerging infection, vaccination, and Guillain-Barré syndrome: a review. Neurol. Ther. 10: 523-537.
17. Kolde R (2010). pheatmap: pretty heatmaps. R package. Available at https://doi.org/10.32614/CRAN.package.pheatmap]
18. Krueger F, James F, Ewels P, Afyounian E, et al. (2023). FelixKrueger/TrimGalore: v0.6.10 - add default decompression path. Zenodo. Available at [https://doi.org/10.5281/ZENODO.7598955].
19. Lazear HM, Govero J, Smith AM, Platt DJ, et al. (2016). A mouse model of Zika virus pathogenesis. Cell Host Microbe. 19: 720-730.
20. Leonhard SE, Mandarakas MR, Gondim FAA, Bateman K, et al. (2019). Diagnosis and management of Guillain-Barré syndrome in ten steps. Nat. Rev. Neurol. 15: 671-683.
21. Liao Y, Smyth GK and Shi W (2014). featureCounts: an efficient general purpose program for assigning sequence reads to genomic features. Bioinformatics. 30: 923-930.
22. Mier-y-Teran-Romero L, Delorey MJ, Sejvar JJ and Johansson MA (2018). Guillain-Barré syndrome risk among individuals infected with Zika virus: a multi-country assessment. BMC Med. 16: 67.
23. Miner JJ and Diamond MS (2017). Zika virus pathogenesis and tissue tropism. Cell Host Microbe. 21: 134-142.
24. Reid S, Rimmer K and Thakur K (2018). Zika virus and neurologic disease. Neurol. Clin. 36: 767-787.
25. Ricklin D, Reis ES, Mastellos DC, Gros P, et al. (2016). Complement component C3 - the "Swiss Army Knife" of innate immunity and host defense. Immunol. Rev. 274: 33-58.
26. Robinson MD, McCarthy DJ and Smyth GK (2010). edgeR: a Bioconductor package for differential expression analysis of digital gene expression data. Bioinformatics. 26: 139-140.
27. Schafflick D, Kieseier BC, Wiendl H and Meyer Zu Horste G (2017). Novel pathomechanisms in inflammatory neuropathies. J. Neuroinflammation. 14: 232.
28. Seqera (n.d.). MultiQC. Available at [https://seqera.io/multiqc/].
29. SRA Toolkit Archives (2021). NCBI Insights. Available at [https://ncbiinsights.ncbi.nlm.nih.gov/tag/sra-toolkit/].
30. Subramanian A, Tamayo P, Mootha VK, Mukherjee S, et al. (2005). Gene set enrichment analysis: a knowledge-based approach for interpreting genome-wide expression profiles. Proc. Natl. Acad. Sci. USA. 102: 15545-15550.
31. Thomas PD, Ebert D, Muruganujan A, Mushayahama T, et al. (2022). PANTHER: making genome-scale phylogenetics accessible to all. Protein Sci. 31: 8-22.
32. Wang X, Yu J and Zhang X (2022). Editorial: Pathogenic microbes: multi-omics analysis of host-pathogen interactions and immune regulation. Front. Cell. Infect. Microbiol. 12: 1053792.
33. Wickham H (2009). ggplot2: elegant graphics for data analysis. 1st edn. Springer, New York.

Supplementary Table S1: Assessment of the potential influence of the PC2-deviating sham replicate

Contrast	Includes PC2-deviating sham replicate?	Potential influence of sham replicate	Primary markers evaluated	Main biological interpretation
Paralyzed vs Sham	Yes	Possible influence because the sham group is part of this contrast	IFIT1, ISG15, CXCL10, STAT1, TNF	Acute inflammatory/paralysis-associated signature
Recovering vs Sham	Yes	Possible influence because the sham group is part of this contrast	PDCD1, CTLA4, CXCR3, CCL5, IL12B, ITGAE	Adaptive recovery footprint compared with baseline sham state
Recovering vs Paralyzed	No	No direct influence because sham samples are not included in this contrast	ARG1, MSR1, CLEC4N, IFI30, TGM2	Recovery/remodeling signature